J Mater Sci (2008) 43:2143–2148
DOI 10.1007/s10853-007-2019-6

ZnO ultra-fine powders and films: hydrothermal synthesis, luminescence and UV lasing at room temperature

Lyudmila Nikolaevna Dem'yanets · Lyudmila Li · Tatiana Uvarova · Yurii Mininzon

Received: 9 November 2006 / Accepted: 20 July 2007 / Published online: 4 October 2007

Abstract Zinc oxide ultra-fine crystalline powders and polycrystalline films of high optical quality were synthesized under soft hydrothermal conditions. The phase composition, crystal morphology, and luminescent properties of submicron ZnO powders and films were studied depending on synthesis conditions (system composition, precursor kind, solvent type and concentration, temperature). For the systems containing metallic zinc, the ZnO growth mechanism was suggested. The most intensive UV luminescence and the highest values of I_{UV}/I_{VIS} were observed for polycrystalline films grown on Zn substrates. Low-threshold UV lasing at room temperature was found for ZnO-films, grown in hydrothermal systems with hydroxide or halide solutions as solvents, E_{th} = 1–5 MW/cm^2. The lowest threshold was observed on the ZnO films grown using LiOH as a solvent and zinc nitrate as ZnO-precursor. Clear mode structures with line-width 0.3 nm are characteristic of the lasing spectra.

Introduction

Zinc oxide is a multifunctional compound, which is intensively studied during last decade. Such interest is defined by the unique physical properties of ZnO. This compound is a direct wide bandgap semiconductor (band gap is 3.37 eV); it has the outstanding for $A^{II}B^{VI}$ binary systems exciton binding energy (60 meV) providing the existence of UV luminescence caused by exciton recombination in a wide temperature range up to 500 °C. Zinc oxide is a functional nanoscaled material belonging to a new class of the monochromic emission sources based on noncavity stimulated emission.

Lasing in ZnO nanostructures has attracting increasing attention in recent years due to an expected low-threshold power density required for lasing [1]. Over the past few years, UV lasing action has been observed in various ZnO objects, such as nanowires and nanoribbons [1–6], nanorods [7], tetrapods [8, 9], films [10–12], powders, [13], ceramics [14].

During the past years various methods and approaches have been developed for synthesis of ZnO low-dimensional crystals. Among them there are the traditional and modified methods of synthesis from liquid, solid, gas phases, such as inorganic and metal-organic chemical vapor deposition CVD [15, 16], MOCVD [17], molecular beam epitaxy MBE [18, 19], mechano-chemical synthesis [20], high temperature pyrolysis [9], Zn-oxidation in vapor or liquid phases [21–23], hydrothermal synthesis [5, 24–27], sol–gel synthesis [28], magnetron sputtering [11, 29].

Among several hundreds of scientific communications concerning ZnO-nanocompounds preparation and properties, only small part describes the generation of stimulated emission in synthesized samples (see, for example [9, 13, 30–34]. It is clear that the efficiency of UV stimulated emission is defined by several factors, such as (a) morphological and dimensional characteristics of individual crystallites, (b) peculiarities of their space arrangement, (c) spectroscopic characteristics of the compound under study (nominally pure or doped one).

To our knowledge, the lasing in hydrothermally grown ZnO nanoobjects has been reported only in two articles [5, 6], although the hydrothermal synthesis is a powerful and promising method for preparing low-dimensional

L. N. Dem'yanets (✉) · L. Li · T. Uvarova · Y. Mininzon
Institute of Crystallography RAS, Leninskii pr.59, Moscow 119333, Russian Federation
e-mail: demianets@ns.crys.ras.ru

compounds due to simple procedure, low cost, low temperatures, and ability to change growth conditions in a wide range, and there are many publications describing the ZnO nanoobjects prepared by this method [5, 6, 24–27, 35–40].

Here we report the data on synthesis and low-threshold lasing in ZnO high optical quality crystalline films grown under soft hydrothermal conditions.

Experimental

Zinc oxide films were grown on seeding plates of poly- or single crystalline metallic Zn. The experimental methods were similar to that described earlier [41]. As-prepared zinc hydroxide or ZnO chemical, $Zn(NO_3)_2 \cdot 6H_2O$, $Zn(CH_3COO)_2 \cdot 2H_2O$ were used as ZnO-precursors; aqueous solutions of LiOH, KOH, NH_4OH, NH_4Cl, KF with concentrations 1–8 mass% were used as solvents. The zinc hydroxide colloid was prepared by adding of the proper quantity of ammonium hydroxide or potassium hydroxide to a zinc acetate or nitrate solutions at room temperature. The polycrystalline Zn-plates were placed vertically in the upper part of Teflon cans (15–40 cm^3 capacity) containing starting chemical components. The reaction duration was 2–48 h at 130–180 °C. The obtained crystalline powders (nutrient) and substrates were washed, filtered and then dried at room temperature.

The films obtained were analyzed by XRD, SEM, and spectroscopic techniques. The composition and structure type of the films was confirmed by X-ray powder diffraction data (Diffractometer Rigaku D-max III-c, λCu Kα). Growth morphology was studied using SEM Philips 515 and JEOL JXA-840, operating at a maximum accelerating voltage 30 kV.

Pulse cathodoluminescence (PCL) was used for preliminary investigation of the end-products of hydrothermal reactions similar to [24, 25]. Room temperature stimulated emission in ZnO was excited by 355-nm, 4-ns third-harmonic pulses from Nd^{3+}:YAG laser. The diameter of laser beam spot was $\sim$1 mm. The exciting laser beam was directed normally to the film surface. Emission from the sample surface was directed via a flexible multi-core silica fiber to the entrance slit of a MS-300 Spectrometer equipped with a CCD array (the spectral resolution was 0.1 mm). The fiber was oriented at the certain angle θ (15–60°) to the film surface. Experimental conditions were similar to conditions described in [9].

Results and discussion

Earlier [24, 25] we have shown that low-dimensional crystalline powders of ZnO may be synthesized under soft hydrothermal conditions using various solvents, ZnO-precursors, and growth parameters. The crystallite sizes, faceting, aspect ratios and spectroscopic characteristics are defined by growth conditions, among them the ZnO-precursor, solvent type and temperature are the most important. In our experiments, the end-products of hydrothermal interaction between starting components have been represented by films grown on Zn-substrates, and polycrystalline powders deposited from growth media during the synthesis process. According to XRD-data, in both cases the final products (films and powders) have been pure ZnO with wurtzite structure type; no additional reflexes have been observed in XRD-patterns of the analyzed samples. The crystallite sizes in the resultant materials varied from $\sim$100 nm till several μm, depending on the synthesis conditions.

If substrate-seed was introduced into the growth system, crystallization processes became controlled additionally by the characteristics of substrate. In our case, the substrate is a metallic Zn plate, and during the growth process it undergoes to partial dissolution and oxidation. As a result, two zones are being formed in the closed space of the autoclave at the starting stages of growth process. In the growth zone (Zn-substrate), the process of ZnO-formation passes through the stages of oxidation (dissolution)—nucleation—growing, while in the dissolution zone (starting nutrient) this process must pass through the stages of dissolution (dehydration)—nucleation—growth. Such initial inhomogeneity of growth conditions results in obtaining the crystallites with different growth morphology and physical properties in the dissolution zone and on the substrate. There were no considerable difference between the morphology and spectroscopic characteristics of ZnO films grown on poly- and single-crystalline Zn-substrates.

Growth morphology of ZnO

Some examples of growth morphologies of crystallites in powders from bottom part of the vessels and growth morphology of films are shown in Figs. 1–3. Images in the left column show the morphology of ZnO-particles in crystallite powders while images in the right column demonstrate the typical growth morphologies of the films grown on Zn-substrates. Growth morphologies of individual crystallites varied from rounded shape-less forms till well-developed prisms, wires, plates etc. depending on growth conditions.

Ultra-thin powders consist of faceted crystallites with different shapes; typical simple crystallographic forms are hexagonal prism $\{10\bar{1}0\}$, positive and negative monohedrons (0001), $(000\bar{1})$, hexagonal pyramid $\{10\bar{1}1\}$; aspect ratios varies from 50 till 0.2 depending mainly on solvent

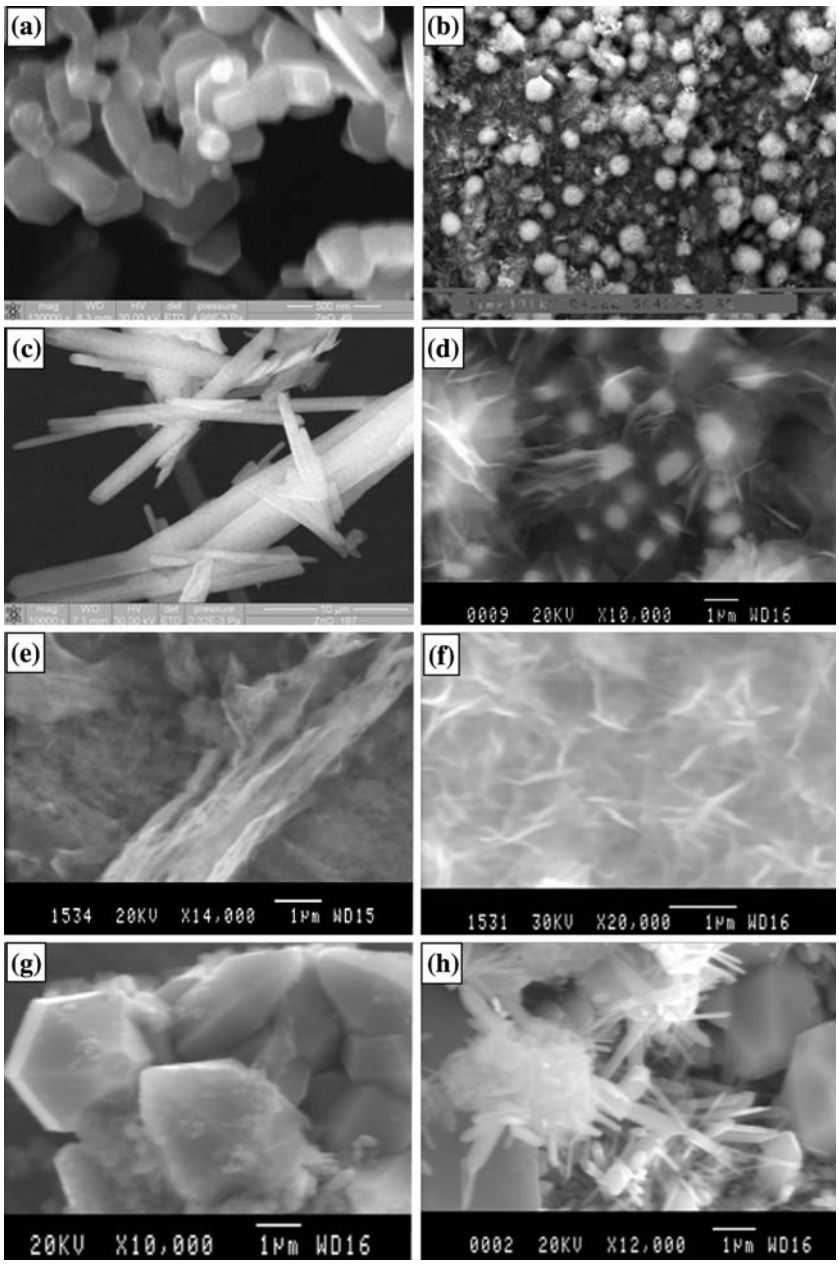

Fig. 1 Growth morphologies of polycrystalline powders (left column) and films on Zn-substrates (right column). (**a**, **b**) #49; ZnO chemical is ZnO-precursor; H_2O is a solvent, 180 °C/48 h; (**c**, **d**) #197; $Zn(NO_3)_2 \cdot 6H_2O$ is ZnO-precursor; NH_4OH 2% is a solvent, 180 °C/10 h; (**e**, **f**) #1020; $Zn(NO_3)_2 \cdot 6H_2O$ is ZnO-precursor; NH_4OH 1% is a solvent, 130 °C/10 h; (**g**, **h**) #193; $Zn(NO_3)_2 \cdot 6H_2O$ is ZnO-precursor; LiOH 3.5 % is a solvent, 180 °C/10 h

type. The crystals with the largest aspect ratios grow in ammonium-containing solutions, Li-ions inhibit the growth rate in *c*-direction; as a result, the crystals with bipyramidal habit are being formed.

At the starting period of hydrothermal treatment, the growth conditions are not uniform even for substrate due to different supply of feeding material to different parts of substrate (edges, corners, surface), and one can find the areas with different morphology along film surface (Fig. 2).

The films consist of ZnO microcrystallites (150–500 nm in size); aspect ratios are from 20 till about 0.02. At the initial stages of crystallization process, prismatic nano-crystals with aspect ratio >1 is forming on the Zn-substrate where the polycrystalline grains serve as the nucleation sites (Fig. 3a). At rather high temperatures, the aligned rows of elongated hexagonal prisms or needle-like crystals are usually formed; *c*-axes of prisms are perpendicular to substrate surface. Then, when furnace is switched out and the autoclaves are slowly cooling up to room temperature, very thin plates grow at the second stage of crystallization process, and the surfaces (more often, the edges) of prismatic crystals provide the nucleation sites for ZnO-plates growing (Fig. 2a, b, right column). Such plates with well-developed {0001} faces are aggregated into flower-like or spherolite-like agglomerates (up to ~10,000 nm); every plate is located in such a way, that [0001] axis is parallel to substrate surface. The typical case is the formation of thin plates on the edges between {0001} and $\{10\bar{1}0\}$ surfaces of

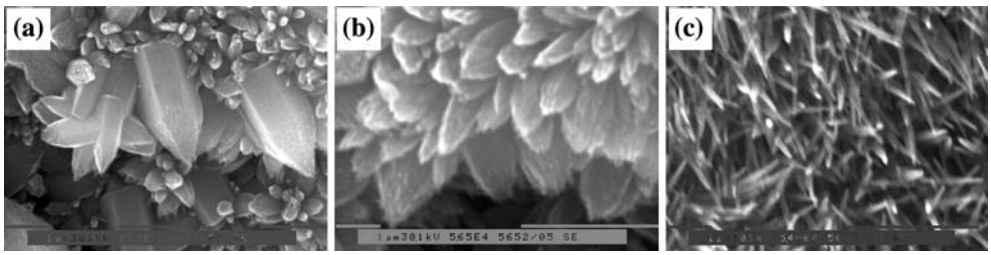

Fig. 2 Growth morphologies of ZnO polycrystalline films in various local sites. (**a**–**c**) #44; $Zn(OH)_2$ is ZnO-precursor; KOH 25 % is a solvent, 180 °C/48 h

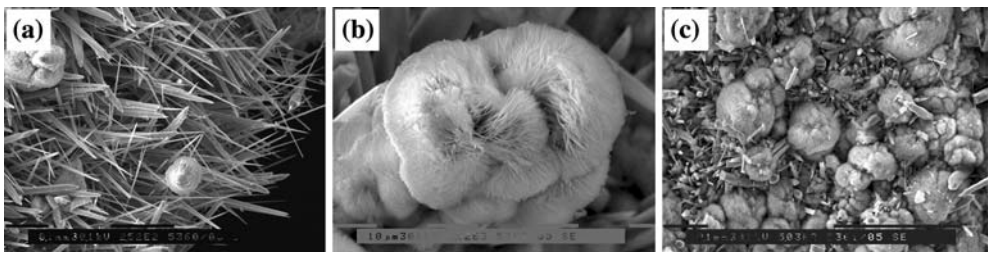

Fig. 3 Growth morphologies of ZnO polycrystalline film at different stages of growth. (**a**–**c**) # 150; $Zn(NO_3)_2 \cdot 6H_2O$ is ZnO-precursor; LiOH 3.4% is a solvent, 180 °C/10 h

the ZnO-prisms, which have been formed during the first stage of the growth process (Fig. 1d, right column). At low growth temperature, the films contain only such thin hexagonal plates with well-developed {0001} monohedrons (Fig. 1f, right column); only hexagonal prisms (the first stage of the growth process) are present on Zn-surface at quenching the autoclave.

Such change in growth mode can be connected with the change of RED/OX potential at the different distances from Zn-substrate, which results in the change of growth mechanism and c/a aspect ratio. At the first stages, an intensive growth of the face of positive monohedron (0001) occurs, $V_{(0001)} \gg V_{(10\ \bar{1}0)}$. Note that positive monohedron face is terminated by Zn-ions; they are in excess on Zn-substrate. Then, after the process of Zn-oxidation on the substrate, the growth, typical for a given solvent and growth conditions, occurs.

Luminescence of ZnO films and powders

Both polycrystalline powders and films were analyzed using pulse cathodoluminescence techniques. Earlier [24, 25] we discussed the PCL spectra of powders and coatings obtained by crystallization in KOH solutions and H_2O. Spectroscopic characteristics for powders and films have been drastically different. In this work we studied also the luminescent characteristics of powders and films obtained in the other solvents (NH_4OH, NH_4Cl, LiOH, and KF). The analysis of PCL spectra has shown that the determined earlier regularities remain valid also for the samples synthesized from these solvents.

Two characteristic bands are usually observed in the spectra of photo- and cathodoluminescence of ZnO powders (Fig. 4). The emission spectra of most ZnO samples show a near-band-edge ultraviolet UV line (band A, $\lambda \sim 375$–385 nm, $\Delta\lambda \sim 20$–12 nm) accompanied by a broad visible deep level luminescence band (band B, $\lambda \sim 520$–620 nm, $\Delta\lambda \sim 60$–220 nm). Band B originates from the various defects depending on growth methods and can decrease the

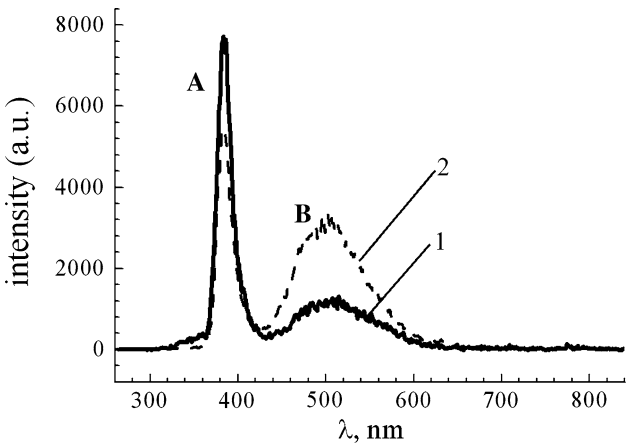

Fig. 4 Spectra of ZnO film registered at photo-(1) and electron-beam (2) excitations (#148-1)

emission efficiency of the UV light devices and increase the lasing emission thresholds. Thus the optical quality of the matter may be evaluated using ratio between the intensities of A and B bands (I_{UV}/I_{VIS}). One can see that the ratio I_{UV}/I_{VIS} is higher for the spectrum of photoluminescence in comparison with cathodoluminescence spectrum due to more effective excitation of deep level centers, which are responsible for emission in VIS region.

Luminescent characteristics of ZnO depend on the growth conditions (type of precursor, solvent, Red/Ox potential) and they are different for powders and polycrystalline films ZnO obtained in the same run. The probable reason of such difference is the appearance of different quenching centers in the crystals obtained at different conditions [24, 25]. Note that luminescence spectra of films and powders are distinct from each other by I_{UV}/I_{VIS}. As a rule, spectra of ZnO films demonstrate strong UV band and very weak band in visible range (or its absence).

To determine the main centers causing the quenching of UV luminescence, we carried out the mathematical treatment of the complicated profiles of luminescence spectra (program t_dn2fb-Ngauss). As an example we have shown the main parameters of components of one complex profile (Fig. 5 and Table 1). Calculations for more then 15 samples have shown that wide VIS-band consists of the series of overlapping bands. The intensities of these bands are strongly dependent on ZnO growth conditions, but at the same time, the intensity of every line varies independently one another. Such behavior allows relating the lines to the centers with different structures. UV-quenching centers are found to radiate mainly in red part of spectrum, $\lambda > 700$ nm.

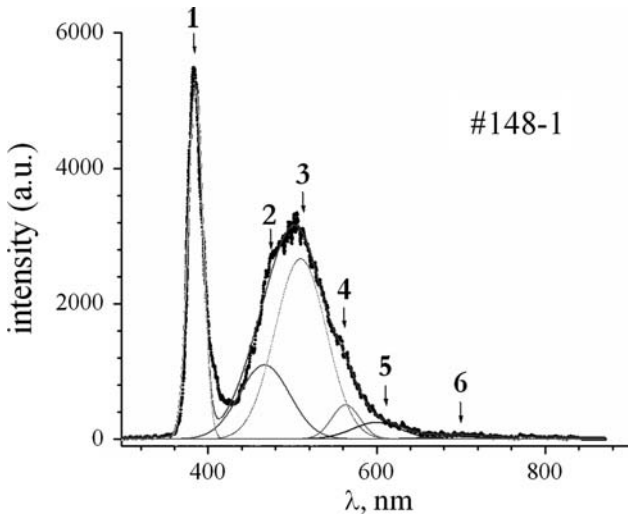

Fig. 5 Mathematical treatment of emission spectrum, shown in Fig. 4(2)

Table 1 Main parameters of the decomposition of the emission spectrum shown in Fig. 5

Number of line	λ (nm)	Square arb.u.*nm *10^5	$\Delta\lambda$ (nm)
1	385.19	1.16	8.93
2	467.0	0.828	30.0
3	510	2.03	30.4
4	563	0.2	17
5	600	0.18	28.8
6	689	0.02	31

Stimulated emission in ZnO films

Basing on our results on ZnO nanocrystal synthesis and preliminary study of luminescence characteristics, for detailed study we have chosen the films obtained on Zn-substrates because these films are characterized by the highest optical quality in accordance with I_{UV}/I_{VIS} evaluations.

Among analyzed ZnO-objects, low-threshold lasing was observed in more than 20 ZnO polycrystalline films. These films were grown from aqueous solutions LiOH 2–5 wt.%, NH_4OH 1–2.5%, NH_4Cl 2.5%, KOH 8–25%, KF 4%, and H_2O. Lasing thresholds of the studied samples varied in the range 4–20 mJ/cm^2. Taking into account the pulse durations (4 ns in our experiments), these values correspond to power density 1–5 MW/cm^2. The lowest thresholds were found for the films synthesized in LiOH, NH_4OH, and KF solutions.

The lasing spectra are characterized by clear mode structure with line-width 0.2 nm. The typical lasing spectrum is shown in Fig. 6 for the ZnO film grown using

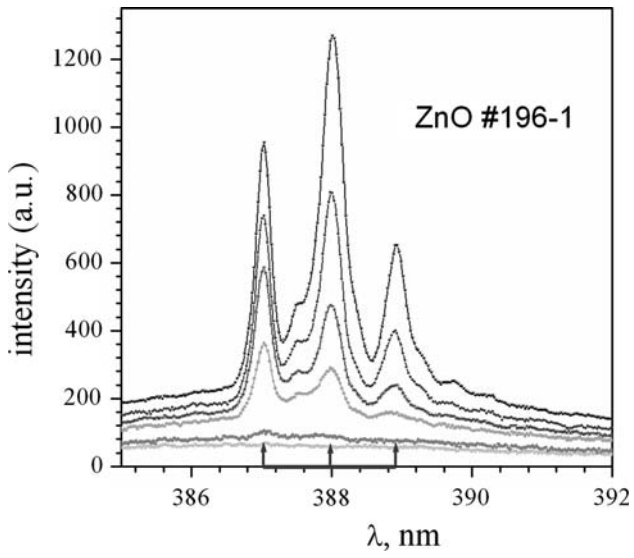

Fig. 6 Emission spectra of ZnO films obtained at varying excitation levels (0.8 E_{th}; E_{th} = 4.8 mJ/cm^2; 1.45 E_{th}; 1.64 E_{th}; 1.95 E_{th}; 2.32 E_{th})

NH_4OH as solvent. Mode spacing $\Delta\lambda \sim 0.94$ nm, and 0.3 nm line-width are characteristic of this spectrum; lasing threshold E_{th} is 4.8 mJ/cm^2. Using simplified equation $L \sim \lambda^2/(2n^*\Delta\lambda)$, where λ is the wavelength, n is refraction index, we have evaluated the resonator length $L \sim 33$ μm.

It should be noted that lasing in hydrothermally grown ZnO was described only in two works [5, 6]. In [6] the conclusion on lasing action was made only on the base of emission line narrowing in $\sim$2 times at the increase of pumping level. The lasing threshold [5] was 70 μJ/cm^2 (280 MW/cm^2) at the excitation by the source with pulse duration 250 fs. This value is much higher than threshold observed in our experiments (1–5 MW/cm^2).

For studied hydrothermally synthesized ZnO powders, the lasing threshold seems to be higher than the power of our laser (5 MW). This fact may be explained by as different optical qualities so as by different morphology of crystallites forming in powders and films.

Resume

Zinc oxide high quality ultra-fine crystalline powders and films were synthesized under soft hydrothermal conditions using aqueous solutions of LiOH, KOH, NH_4OH, NH_4Cl, and KF as solvents. The phase composition, crystal morphology, and luminescent properties of submicron ZnO powders and polycrystalline films were studied depending on synthesis conditions (system composition, precursor kind, solvent type and concentration, temperature and duration of hydrothermal treatment).

The crystallite sizes in the resultant powder materials varied from 100 nm to 10 μm, depending on the synthesis conditions. Growth morphologies varied from rounded shape-less forms till well-developed prisms, wires, plates, flowers etc. Well-aligned ZnO nanorod arrays were characteristic of polycrystalline films grown on Zn-substrates. ZnO microcrystallites were 150–500 nm in size.

Zinc oxide polycrystalline films demonstrated UV lasing at room temperatures, threshold being equal to 1–5 MW/cm^2. The minimal threshold was observed for the ZnO films grown using LiOH solutions. Clear mode structure with line-width 0.3 nm is characteristic of the lasing spectra.

Acknowledgements This work was supported by Russian Foundation for Basic Researches, Grant N 06-02-17230, and by the Federal Program FASI, No. 02.434.11.2017.

References

1. Xuang MH, Mao S, Feick H, Yan Y, Wu Y, Kind H, Weber E, Russo R, Yang P (2001) Science 292:1897
2. Johnson JC, Yan H, Yang P, Saukally RJ (2003) J Phys Chem B 107:8816
3. Liu C, Zapien JA, Yao Y, Meng X, Lee CS, Fan S, Liftshitz S, Lee ST (2003) Adv Mater 15:838
4. Bando K, Awabe T, Asaka K, Masumoto Y (2004) J Phys Chem B 108:358
5. Qui Z, Wong KS, Xu H (2004) Appl Phys Lett 84:2739
6. Choy J-H, Jang E-S, Won J-H, Chung J-H, Jang D-J, Kim Y-W (2004) Appl Phys Lett 84:287
7. Yu SF, Yen C, Lau SP, Park WL, Yi GC (2004) Appl Phys Lett 84:3241
8. Zharko JM, Song JK, Blackledge CW, Swart I, Leone SR, Li S, Zhao Y (2005) Chem Phys Lett 404:171
9. Li LE, Dem'yanets LN, Nikitin SV, Lavrikov AS (2006) Quantum Electron 36:233
10. Tang ZK, Awasaki M, Ohtomo A, Koinuma H, Segawa Y (2006) J Crystal Growth 287:169
11. Yao Z, Zhang X-Q, Shang H-K, Eeng X-Y, Wang Y-S, Huang S-H (2005) Chin Phys 14:1205
12. Bagnal DM, Hen YF, Zhu Z, Yao T, Shen MY, Goto T (1998) Appl Phys Lett 73:1038
13. Cao H, Xu JY, Seeling H, Chang RPH (2000) Appl Phys Lett 76:2997
14. Sun Y, Ketterson JB, Wong GKL (2000) J Appl Phys 77:2322
15. Umar A, Lee S, Im YH, Hahn YB (2005) Nanotechnology 16:2462
16. Han JY, Kim J, Stucky GD (2000) Chem Mater 12:2068
17. Liu S, Wu JJ (2002) Mater Res Soc Symp Proc 241:703
18. Sun X, Geng Z, Li Y (2003) Mater Chem Phys 80:366
19. Bagnal DM, Chen YF, Shen MY, Zhu Z, Goto T, Yao T (1998) J Crystal Growth 184/185:605
20. Shen L, Guo L, Bao N, Yanagisawa K (2003) Chem Lett 32:826
21. Chen Z, Shan Z, Li S, Liang CB, Mao SX (2004) J Crystal Growth 265:482
22. Kwok M, Djurišić AB, Leung YH, Chan WK, Phillips DL, Chen HY, Wu CL, Gwo S, Xie MH (2005) Chem Phys Lett 412:141
23. Wang X, Li Q, Liu B, Zhang J, Liu ZF, Wang R (2004) Appl Phys Lett 84:4941
24. Dem'yanets LN, Li LE, Uvarova TG, Mininzon YM, Briskina CM, Zhilicheva OM, Titkov SV (2004) Inorg Mater 40:1173
25. Dem'yanets LN, Li LE, Uvarova TG (2006) J Crystal Growth 287:23
26. Guo M, Diao P, Cai S (2005) J Solid State Chem 178:1864
27. Sun M, Chen X, Deng ZX, Li YD (2003) Mater Chem Phys 78:99
28. Lee J-H, Ko K-H, Park BO (2003) J Crystal Growth 247:119
29. Chiou W-T, Wu W-Y, Ting J-M (2003) Diamond Relat Mater 12:1841
30. Cao H, Zhao YG, Ho ST, Seelig EW, Wang QH, Chang RPH (1999) Phys Rev Lett 82:2278
31. Thareja RK, Mitra A (2000) Appl Phys B 71:181
32. Bagnall DM, Chen YF, Zhu Z, Yao T, Koyama S, Shen MY, Goto T (1997) Appl Phys Lett 70:2230
33. Yu SF, Clement Y, Lau SP, Lee HW (2004) Appl Phys Lett 84:3244
34. Kwok WM, Djurišić AB, Leung YH, Chan WK, Phillips DL (2005) Appl Phys Lett 87:223111
35. Zhao Y, Kwon Y-U (2004) Chem Lett 33:1578
36. Wei A, Sun XW, Xu CX, Dong ZL, Yu MB, Huang W (2006) Appl Phys Lett 88:213102
37. Sun XM, Chen X, Deng ZX, Li YD (2003) Mater Chem Phys 78:99
38. Liu B, Zeng HC (2003) J Am Chem Soc 125:4430
39. Li W-J, Shi E-W, Zhong W-Z, Yin Z-W (1999) J Crystal Growth 203:186
40. Guo M, Diao P, Wang X, Cai S (2005) J Solid State Chem 178:3210
41. Dem'yanets LN, Ivanov-Shitz AK, Li LE, Uvarova TG (2004) Tranc Mat Res Soc Japan 29:2353